Heat Mass Transfer (2007) 43:1273–1281
DOI 10.1007/s00231-006-0213-8

ORIGINAL

Flow and heat transfer analysis in porous wick of CPL evaporator based on field synergy principle

Z. C. Liu · W. Liu · A. Nakayama

Received: 8 January 2006 / Accepted: 1 December 2006 / Published online: 4 January 2007

Abstract In order to optimize the structure of a CPL evaporator and enhance heat transfer, a mathematical and physical model is developed to analyze the flow and heat transfer in the porous wick of the evaporator, whose calculation domain is divided into two parts: vapor-saturated region and liquid-saturated region. The characteristics of flow and heat transfer in the porous wick of a CPL evaporator have been numerically studied according to the field synergy principle. The influences of geometrical structures and heat flux on heat transfer enhancement are analyzed and illustrated by the figures in the present paper.

List of symbols

c	specific heat (J kg^{-1} K^{-1})
h_{fg}	latent heat of evaporation (J kg^{-1})
K	wick permeability (m^2)
L_x	total wick length in x direction (m)
L_{xf}	heated wick length in x direction (m)
L_y	wick length in y direction (m)
p	pressure (Pa)
q	heat flux (W m^{-2})
Q	heat load (W)
R_g	gas constant (J kg^{-1} K^{-1})
r	effective capillary radius of wick pore (m)
t	time (s)
T	temperature (°C)
u	velocity in x direction (m s^{-1})
$\vec{V}$	velocity vector (m s^{-1})
v	velocity in y direction (m s^{-1})
x, y	coordinates (m)
$\vec{n}$	outward normal vector

Greek symbols

α	heat transfer coefficient (W m^{-2} K^{-1})
θ	synergy angle (°)
λ	thermal conductivity (W m^{-1} K^{-1})
ϕ	wetting angle (°)
μ	viscosity (Pa s)
ρ	density (kg m^{-3})
σ	liquid–vapor surface tension (N m^{-1})
ε	phase content

Subscripts

c	condenser
eff	effective
i	index to identify vapor or liquid
in	inlet
l	liquid
s	solid
sat	saturation
v	vapor
rf	reference
0	initial state
∞	vapor in groove

Z. C. Liu · W. Liu (✉)
School of Energy and Power Engineering,
Huazhong University of Science and Technology,
Wuhan 430074, People's Republic of China
e-mail: w_liu@hust.edu.cn

A. Nakayama
Department of Mechanical Engineering,
Shizuoka University, 3-5-1 Johoku,
Hamamatsu 432-8561, Japan

1 Introduction

With the increasing of heat load in satellite or spacecraft systems, waste heat dissipation in these systems becomes a more and more challenging task for thermal scientists and engineers. Two-phase heat transfer devices with capillary pumping of a working fluid are of particular interest in thermal control applications of satellite or spacecraft because of the high heat transfer capacity associated with phase change. The capillary pumped loop (CPL) is one of these advanced two-phase devices which utilize the phase change of working liquid to transfer heat.

The major components of a typical CPL include evaporator, condenser, reservoir, vapor and liquid lines. For the normal operation, heat is transferred to the evaporator, which makes the working fluid evaporate. The working vapor carries heat to the vapor line and the condenser, and heat is then removed in the condenser by the heat sink. Then the condensed liquid is transferred to the liquid line and the evaporator by the capillary force caused by the curvature of the vapor–liquid interface. The control of temperature or pressure of CPL reservoir determines the loop pressure and saturation temperature.

Recently capillary pumped loops have been under intensive investigation for space application and electronic cooling in many countries [1–3]. Numerous CPLs have been designed, fabricated and ground-tested. Several designs have been successfully tested in flight experiments so that some of them have been selected for space thermal application [1, 2]. Experimental researches have shown that when a CPL works, temperatures and pressures may oscillate, and its operation at low heating loads is particularly prone to fluctuations [4, 5]. CPL equipment is likely to fail if these oscillations become large. In order to reduce pressure and temperature oscillations in CPL, a condenser containing a porous structure was proposed by Muraoka et al. [5], who performed theoretical and experimental studies by employing a plane condenser with a wick. They concluded that these structures can reduce or eliminate the pressure oscillations, and then improve the operating performance of CPL.

The capillary force, which is derived from the meniscus formed at the liquid–vapor interface of the porous wick in the evaporator, is the main force to drive the working fluid, so the evaporator is the most important part of CPL. The better understanding of evaporator performance is crucial to design a CPL system. Cao and Faghri [6] presented a conjugate analysis of a flat-plate type evaporator, in which the porous wick is liquid-saturated, and the evaporation takes place only on the interface of porous wick. The research of Demidov et al. [7] showed that the evaporation could take place within the porous wick, and their mathematical model was derived on the basis of Darcy's law. Figus et al. [8] studied the heat and mass transfer in the porous wick of an evaporator with a Darcy model and a pore network model. LaClair and Mudawar [9] performed a thermal transient analysis for a fully-flooded cylindrical capillary evaporator subject to uniform heat flux prior to the initiation of boiling, and the results were obtained by adopting the Green's function method.

A CPL is a device with a variable overall effective thermal conductivity. The heat transferred from the evaporator with high temperature to the the condenser with low temperature depends directly on the overall effective thermal conductivity of the CPL, which is a combination of conduction and convection. It is clear that, the overall effective thermal conductivity is variable and it depends directly on the fluid circulation. Therefore, to increase the overall effective thermal conductivity, one has to increase the mass flow rate and reduce the flow resistance in the loop.

As the evaporator is the key component of the CPL system, researchers have paid much attention to the study of flow and heat transfer in the evaporator. Some experimental and simulation investigations about CPL evaporators have been conducted and some achievements have also been obtained. However, there is no one who studies heat transfer enhancement in the CPL evaporator and provides guidance to optimize the configuration of the evaporator.

To solve the problem above, Guo et al. [10] proposed a novel concept, called field synergy principle, for enhancing convective heat transfer. They pointed out that convective heat transfer can be effectively enhanced by reducing the synergy angle between temperature gradient and velocity vector. Tao et al. [11] extended this theory to elliptic fluid flow and other transport phenomena, and gave a numerical verification. Shen and Liu extended the field synergy principle to natural convective heat transfer with phase change in porous media [12]. In this paper, the numerical simulation method based on the field synergy principle is introduced to analyze the effect of heat flux and geometrical structures on flow and heat transfer in the porous wick of evaporator, and propose a novel method to enhance heat transfer in a CPL evaporator.

2 Mathematical analysis

A flat-plate evaporator is studied in this paper. The surface of evaporator wall is grooved to remove the vapor. The porous wick to generate the capillary force is made of stainless steel wire mesh. The heat flux is applied on the top wall of the evaporator. Methanol is assumed as the working fluid. Figure 1 schematically shows the present CPL system. The evaporator can be divided into a number of symmetric segments. One is shown in Fig. 2. In the calculation, an assumption is made that the methanol liquid can be continuously provided and its inlet temperature is constant.

To establish the mathematical model, some further assumptions have been made as: (1) porous matrix is incompressible, homogeneous and isotropic; (2) porous wick, liquid and vapor are in local thermal equilibrium; (3) vapor pressure in the porous wick is saturated pressure; (4) gravity and buoyancy can be ignored. Subject to mass, momentum and energy conservation, the volumetric averaging technique is introduced to obtain the mathematical model [13, 14] in the liquid-saturated region and the vapor-saturated region separately. The flow in porous wick is modeled by the Brinkman–Forchheimer extended Darcy model. The averaged mass, momentum and energy conservation equations are as follows.

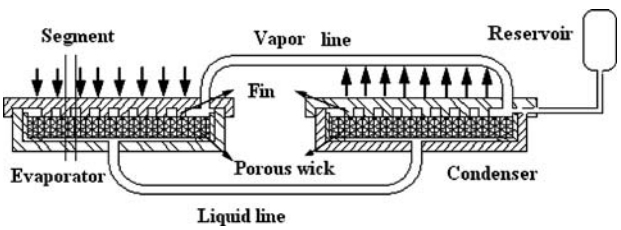

Fig. 1 Scheme of a flat-plate CPL

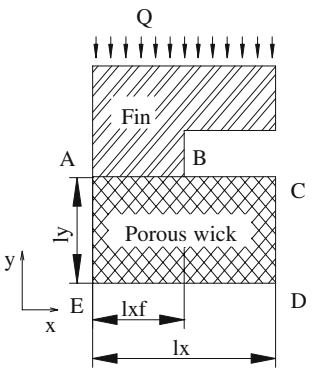

Fig. 2 Computational segment of evaporator (ABCDE)

Mass conservation equation:

$$\frac{\partial(\varepsilon_i\rho_i)}{\partial t}+\nabla\cdot\left(\rho_i\vec{V}_i\right)=0 \tag{1}$$

Momentum equation:

$$\frac{\rho_i}{\varepsilon_i}\frac{\partial\vec{V}_i}{\partial t}+\frac{\rho_i}{\varepsilon_i^2}\left(\vec{V}_i\cdot\nabla\right)\vec{V}_i = -\nabla P_i-\left[\frac{\mu_i}{K_i}+\frac{\rho_i C}{\sqrt{K}}\left|\vec{V}\right|\right]\vec{V}_i+\frac{\mu_i}{\varepsilon_i}\nabla^2\vec{V}_i \tag{2}$$

Energy equation:

$$\overline{\rho c}\frac{\partial T}{\partial t}+\rho_v c_v\left(\vec{V}_v\cdot\nabla\right)T+\rho_l c_l\left(\vec{V}_l\cdot\nabla\right)T=\nabla\cdot(\lambda_{\text{eff}}\nabla T) \tag{3}$$

Above equations can be used in both vapor-saturated and liquid-saturated regions:

$$\begin{cases} i=v & \text{vapor} \\ i=l & \text{liquid} \end{cases} \tag{4}$$

The equations for the two regions are coupled in the calculation. Averaged product $\overline{\rho c}$ and effective thermal conductivity λ_{eff} are as follows.

$$\overline{\rho c}=\left[\rho_l c_l\varepsilon_l+\varepsilon_v\rho_v c_v\right]+(1-\varepsilon_s)(\rho c)_s \tag{5a}$$

$$\lambda_{\text{eff}}=(\varepsilon_l\lambda_l+\varepsilon_v\lambda_v)\varphi+(1-\varphi)\lambda_s \tag{5b}$$

To solve the equations, we have the following conditions.

Initial distribution of liquid content:

$$\varepsilon_l(t=0)=0.611 \tag{6}$$

Bottom boundary (y=0):

$$p_l=p_0,\quad T_l=T_0 \tag{7}$$

Symmetry boundary ($x=0$, $x=l_x$):

$$\frac{\partial p}{\partial x}=0,\quad \frac{\partial T}{\partial x}=0 \tag{8}$$

Top boundary ($y=l_y$, $x<l_{xf}$):

$$\frac{\partial p}{\partial y}=0,\quad \lambda_{\text{eff}}\frac{\partial T}{\partial y}=q_w \tag{9}$$

Top boundary ($y=l_y$, $l_{xf}<x<l_x$):

$$\lambda_{\text{eff}}\frac{\partial T}{\partial y}=\alpha(T-T_\infty),\quad \lambda_{\text{eff}}\frac{\partial T}{\partial y}=\frac{\rho_l h_{fg}K}{\mu_l}\frac{\partial p}{\partial y} \tag{10}$$

For the liquid–vapor phase interface, we have the following conditions.

Temperature continuum:

$$T_{\mathrm{l}} = T_v = T_{\mathrm{sat}} \tag{11}$$

Energy conservation:

$$\lambda_v \nabla T_v \cdot \vec{n} - \lambda_{\mathrm{l}} \nabla T_{\mathrm{l}} \cdot \vec{n} = \rho_{\mathrm{l}} \vec{V}_{\mathrm{l}} \cdot \vec{n} h_{fg} \tag{12}$$

Mass conservation:

$$\rho_{\mathrm{l}} \vec{v}_{\mathrm{l}} = \rho_v \vec{V}_v \tag{13}$$

Force equilibrium:

$$p_{\mathrm{c}} = p_v - p_{\mathrm{l}} = 2\sigma \cos\varphi / r \tag{14}$$

From the Clausius–Clapeyron equation:

$$p_{\mathrm{l}} = p_{rf} \exp\left[-\frac{h_{fg}}{R_g}\left(\frac{1}{T_{\mathrm{l}}} - \frac{1}{T_{rf}}\right)\right] \tag{15}$$

3 Field synergy principle for heat transfer enhancement

In this study, attention has been paid to the heat transfer enhancement based on the synergy between temperature field and velocity field, and unsteady item has been omitted to simplify the derivation. Assuming the steady-state conditions, integrating Eq. 2 over the computation domain shown in Fig. 2 and incorporating the Gauss Law of reduction of integral dimensionality for the diffusion term, the terms FM and HD can be expressed as follows to represent convection and conduction respectively.

$$\begin{aligned}
\mathrm{FM} &= \iiint_{\Omega=ABCDE} \rho_v c_v (\vec{v} \cdot \nabla T)\mathrm{d}x\mathrm{d}y \\
&+ \iiint_{\Omega=ABCDE} \rho_{\mathrm{l}} c_{\mathrm{l}} (\vec{V} \cdot \nabla T)\mathrm{d}x\mathrm{d}y \\
&= \iiint_{\Omega=ABCDE} \rho_v c_v \left|\vec{V}\right| \cdot |\nabla T| \cos\theta_{\vec{V}_v,\nabla T}\mathrm{d}x\mathrm{d}y \\
&+ \iiint_{\Omega=ABCDE} \rho_{\mathrm{l}} c_{\mathrm{l}} \left|\vec{V}\right| \cdot |\nabla T| \cos\theta_{\vec{V}_v,\nabla T}\mathrm{d}x\mathrm{d}y
\end{aligned} \tag{16}$$

$$\begin{aligned}
\mathrm{HD} &= \iiint_{\Omega=ABCDE} [\nabla \cdot (\lambda_{\mathrm{eff}} \nabla T)]\mathrm{d}x\mathrm{d}y \\
&= \oint_{\Gamma=ABCDE} (\vec{n} \cdot \lambda_{\mathrm{eff}} \nabla T)\,\mathrm{d}S
\end{aligned} \tag{17}$$

So the Eq. (3) can be rewritten as

$$\begin{aligned}
&\oint_{\Gamma=ABCDE} (\vec{n} \cdot \lambda_{\mathrm{eff}} \nabla T)\mathrm{d}S \\
&- \iiint_{\Omega=ABCDE} \Big(\rho_v c_v |\vec{V}| \cdot |\nabla T| \cos\theta_{\vec{V}_v,\nabla T} \\
&+ \rho_{\mathrm{l}} c_{\mathrm{l}} |\vec{V}| \cdot |\nabla T| \cos\theta_{\vec{V}_{\mathrm{l}},\nabla T}\Big)\mathrm{d}x\mathrm{d}y = 0
\end{aligned} \tag{18}$$

where $\vec{n}$ represents the outward normal vector along each boundary and dS is the length differential of boundary. In the left side of Eq. 18, the first term is the conductive heat flux in the calculation domain and the second term is the convective heat source. $\theta_{\vec{V}_v,\nabla T}$ is the synergy angle between vapor velocity and temperature gradient and $\theta_{\vec{V}_{\mathrm{l}},\nabla T}$ is the synergy angle between liquid velocity and temperature gradient. According to the field synergy principle [10, 11], the convective heat transfer can be expressed as conductive heat transfer with an internal heat source, and the convective term FM can be looked at as equivalent heat source. Based on this principle the convection can be enhanced through a source enhancement. In this principle the equivalent heat source is dependent not only on the physical properties and fluid velocity, but also the synergy angle between velocity vector and temperature gradient. By reducing this angle, the heat transfer can be enhanced.

The synergy angle can be obtained as

$$\cos\theta = \frac{\vec{V} \cdot \nabla T}{\left|\vec{V}\right| \cdot |\nabla T|} \tag{19}$$

The average synergy angle of the whole calculation domain is

$$\theta_m = \frac{\sum A_{\mathrm{i}} \theta_{\mathrm{i}}}{\sum A_{\mathrm{i}}} \tag{20}$$

where A_{i} represents the area of each computation element. According to Guo et al. [10], the smaller the synergy angle, the better of the synergy between heat transfer and fluid flow, and the more efficient the heat transfer device.

4 Solution scheme

The governing equations are discretized in all regions using a finite volume method. The SIMPLE algorithm is adopted to deal with the linkage between pressure and velocity and the power-law scheme is used to discretize convective and conductive terms. The interface

tracking method is used to track the position of moving phase-change interface. Computations with a staggered grid in primitive variables and alternating direction iterative (ADI) technique are adopted to solve the coupled linear equations. In order to ensure the convergence of calculating procedure, some technical treatments like under-relaxation and additional source are adopted. The mesh grid of the domain is chosen to be uniform in x and y direction. In order to obtain a mesh-independent result, different grid number, such as 25 × 25, 30 × 30 and 40 × 40, are adopted during the numerical simulation. The result proves that a 30 × 30 mesh grid size is adequate.

5 Results and discussions

The convergence of the numerical process was examined by checking the mass and energy balances. The calculation data are obtained with methanol as the working fluid.

The permeability of capillary wick is $K = 1.869 \times 10^{-10} m^2$. The physical properties are $\lambda_s = 27$W/(m K), $\lambda_l = 0.206$W/(m K), $\lambda_v = 0.0172$W/(m K), $\mu_l = 3.56 \times 10^{-4}$ kg/(m s), $\mu_v = 1.14 \times 10^{-5}$ kg/(m s), $h_{fg} = 1.12 \times 10^6$ J/kg. The geometric parameters are $l_x = 5 \times 10^{-3}$ m, $l_y = 5 \times 10^{-3}$ m.

5.1 Effect of heat flux

Figures 3, 4, 5, 6, 7 and 8 show the temperature field, velocity vector field and synergy angle distribution for $q = 10$ kW/m^2 and $q = 15$ kW/m^2 for the case that evaporator is operating at a steady-state condition. For the figures of velocity vector field, the maxium velocity value of liquid and vapor is 2.2×10^{-6}m/s and 1.3×10^{-4} m/s, respectively. For the temperature profile it can be seen that from the liquid inlet (E–D) to the position near the fin (A–B) the temperature increases gradually, and at the liquid inlet the temperature is uniform. As indicated in these figures the liquid velocity near the inlet is uniform along the flow direction and there is a gradual increase in liquid velocity from the liquid inlet of to the phase change interface. The reason is that the liquid evaporates on the phase change interface, and to maintain the steady evaporation, the liquid must be supplied timely, so the liquid velocity increases from the bottom of the wick to the evaporative font. The vapor velocity increases as the vapor travels from the phase change interface to the vapor channel due to the mass rate increase at the liquid–vapor interface. The evolution of the liquid–vapor interface can be seen from Figs. 3 and 6. The

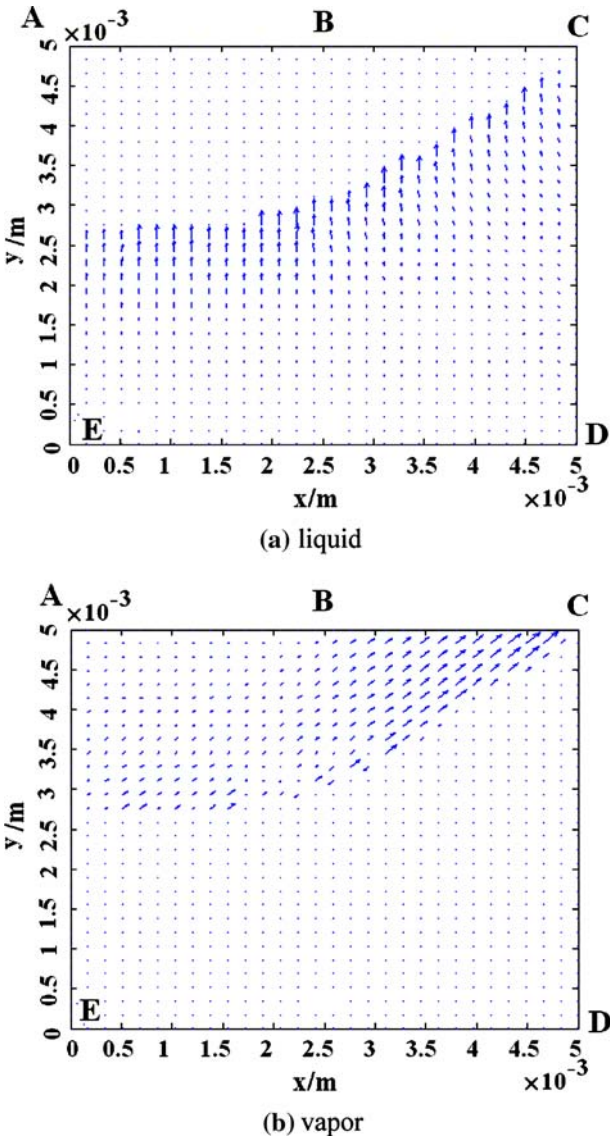

Fig. 3 Velocity vector in evaporator porous wick at heat flux $q = 10$ kW/m^2: **a** liquid; **b** vapor

pumping force of the CPL is the capillary force, $\Delta p_c = \frac{2\sigma \cos \varphi}{r}$, which is developed at the phase change interface. When the heat load increases, ϕ changes correspondingly, which results in a change of Δp_c. When the heat load keeps on increasing, the liquid–vapor interface moves downward to maintain the operating of the CPL. So the liquid–vapor interface in Fig.6 is somewhat lower than that in Fig. 3.

From the figures it can also be found that at the position of the liquid inlet the velocity and the isotherms are almost perpendicular to each other, which indicates that the velocity vector is nearly parallel to the temperature gradient. From the point of view of field synergy principle, under this condition, velocity and temperature gradient have a good synergy ($\theta \approx 0°$). The

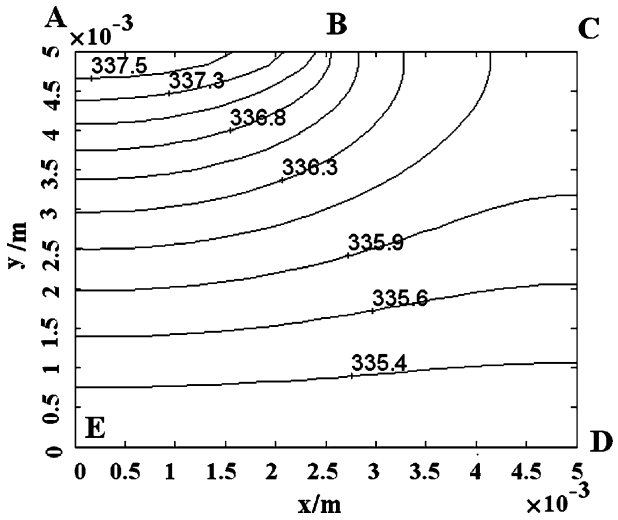

Fig. 4 Isotherms with q = 10 kW/m^2

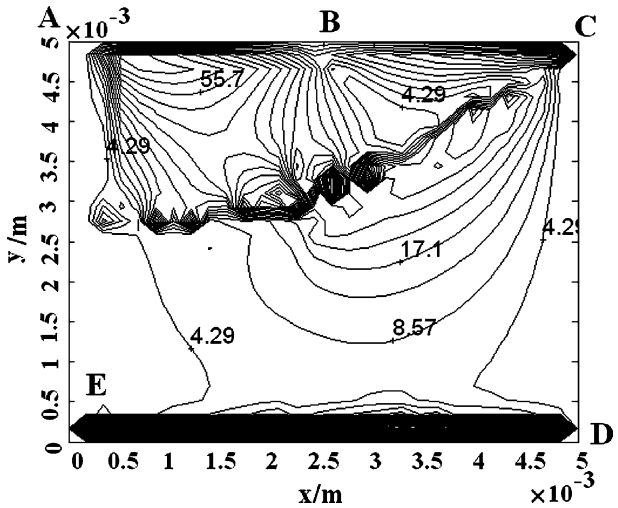

Fig. 5 Distribution of synergy angle with q = 10 kW/m^2

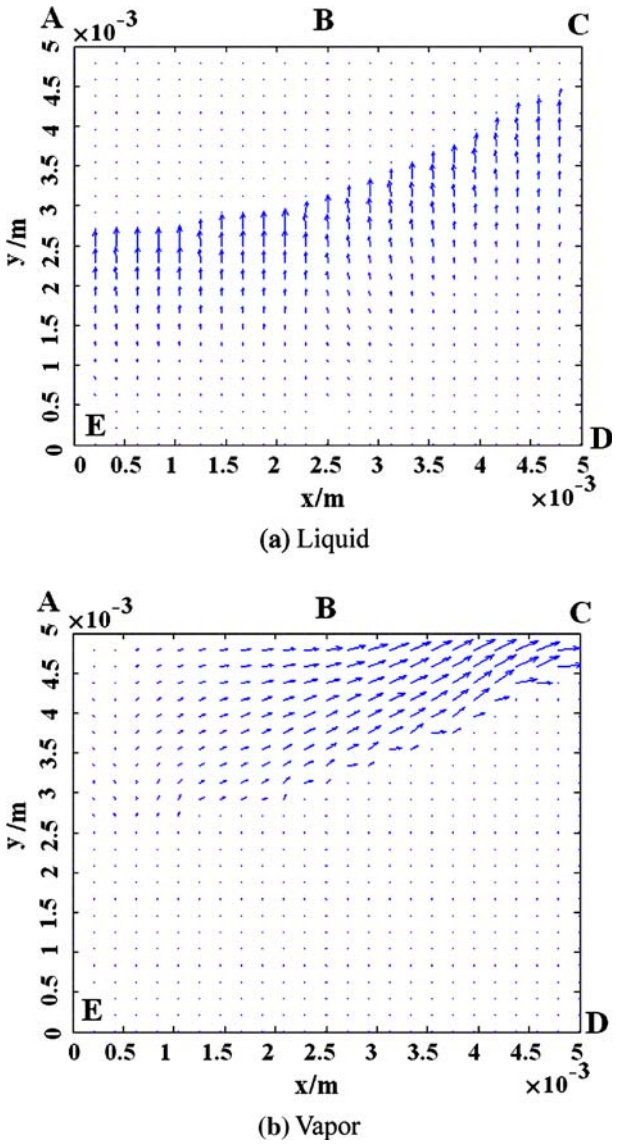

Fig. 6 Velocity vector of evaporator porous wick at heat flux q = 15 kW/m^2: **a** liquid; **b** vapor

synergy angle distribution is provided in Fig. 5. It can be seen that the synergy angles are small in the liquid zone and on the phase change interface, and the heat transfer is enhanced correspondingly. Comparing q = 15 kW/m^2 with q = 10 kW/m^2, the synergy between temperature gradient and velocity vector is better, and thus heat transfer performance is better than the latter. The temperature change in the startup of CPL is shown in Fig.9. During startup, the liquid temperature increases continuously. When startup is accomplished, the temperature remains approximately constant. The change of average synergy angle in the whole domain during startup is provided in Fig. 10. The average synergy angle in the whole domain decreases during the startup and once startup is accomplished it remains nearly constant. The capillary force derived from the liquid/vapor phase change interface is the main force which drives the working fluid in the CPL. The heat flux can affect the position of liquid/vapor interface. The higher the heat flux, the lower the position of the interface, which implies that the fluid flow status is largely related to the heat flux. As shown in Fig. 10, at the beginning of startup the synergy angle is large, which means the heat transfer at that time is not enhanced. With time going on, the synergy angle decreases rapidly, that is to say the fluid flow and the temperature gradient have a good synergy. Once startup is accomplished and the evaporator operates stably, the temperature and velocity fields no longer

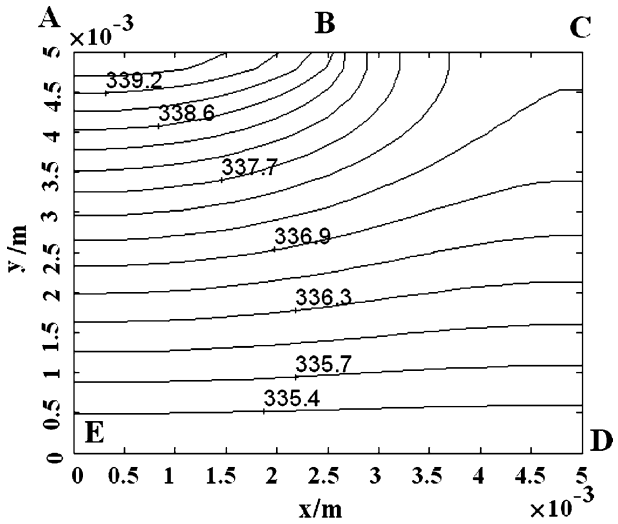

Fig. 7 Isotherms with q = 15 kW/m^2

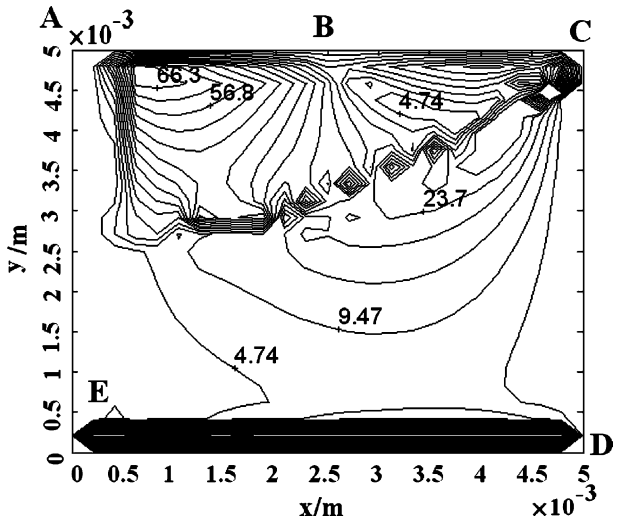

Fig. 8 Distribution of synergy angle with q = 15 kW/m^2

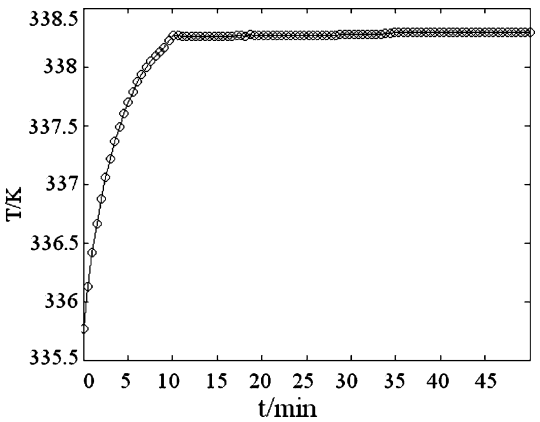

Fig. 9 Outlet temperature versus time for q = 15 kW/m^2

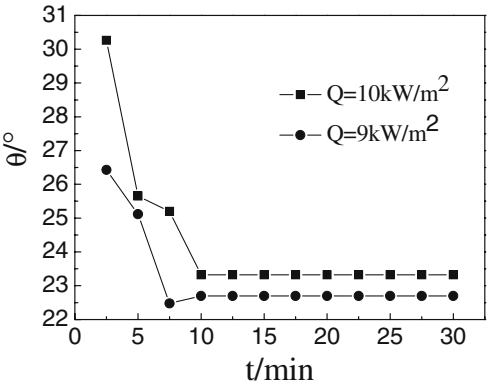

Fig. 10 Average synergy angle versus time

change. Thus the average synergy angle is stable in the whole domain.

Figure 11 shows the heat flux effect on the outlet vapor temperature, where the temperature varies with the heat load 15–30–15 kW/m^2. The CPL has a relatively fast response to heat flux changes within relavively short transients until it reaches a steady state again. Fig. 12 shows the relation of the average synergy angle with the heat flux. It can be observed that with an increase of heat flux, the average synergy angle decreases to a minimum value and then increases. The heat flux from the fin to the upper surface of the porous wick is transferred: (1) to the porous wick by conduction, (2) to the vapor groove by liquid phase change and vapor flow. High heat flux results in an increase of vapor velocity, and also increases the heat convection. Under low heat flux, the evaporation of the liquid is weak and the vapor flow rate is small, which results in a weak convective heat transfer. When heat flux is increased, the evaporation of the working fluid is enhanced, which boosts up the flow of fluid through the porous wick, so the convection is intensified and the synergy of flow and heat transfer is improved. When heat flux q = 18 kW/m^2, the average synergy angle in the whole domain reaches a minimum value, 20.925°, at this point heat transfer of the evaporator reaches the maximum according to the field synergy principle, and this means physically that dryout is reached. Thereafter, the increasing heat flux leads to an increasing synergy angle. Liao and Zhao [15] experimentally study the evaporative heat transfer in a capillary structure heated by a grooved block, and their experimental results showed that with an increase of the imposed heat flux, the heat transfer coefficient increases to a maximum value and then decreases afterwards. So these results are consistent with the conclusions in reference [15].

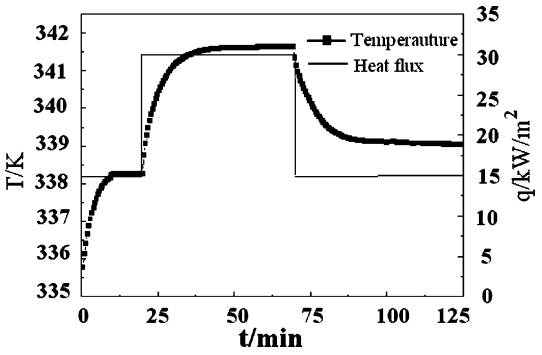

Fig. 11 Transient outlet temperature and heat flux density

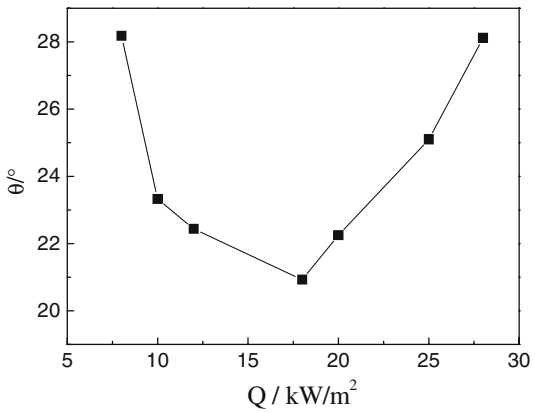

Fig. 12 Average synergy angle versus heat flux density

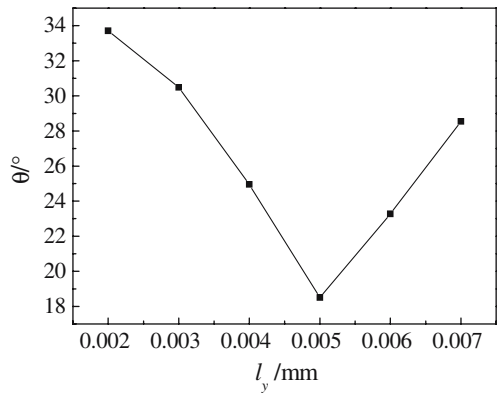

Fig. 13 Average synergy angle versus thickness of porous wick, 15 kW/m^2

5.2 Effect of thickness of porous wick

Figure 13 shows the variation of average synergy angle with the thickness of porous wick for heat flux density q = 15 kW/m^2. It can be clearly observed that with an increase of porous wick thickness, the average synergy angle reduces to a minimum value and then increases.

The total energy balance for the fluid flow through the porous wick can be written as

$$Q = \dot{m} \cdot h_{fg} + \dot{m} c_{pl}(T_v - T_c) \tag{21}$$

where $\dot{m}$ is the mass flow rate of fluid, T_v is the saturation temperature of vapor, $T_c$is the inlet temperature of liquid, $c_{pl}$is the specific heat of liquid, $h_{fg}$is the latent heat of vaporization. The first term of right hand of Eq. 21 represents the latent heat, while the second term represents the sensible heat. As mentioned above, the heat flux imposed on the upper surface of the wick is transferred by conduction, vapor convection and phase change on the liquid/vapor interface. In a porous wick at small thickness the temperature profiles are curved towards the heating fin and the synergy angle of liquid velocity vector and temperature gradient is large, that is the heat transfer is not synergized perfectly with the liquid flow. With the increase of porous wick thickness, the temperature and liquid velocity fields in porous wick become in good synergy, so the heat transfer ability is greatly improved. But when the thickness of porous wick increases further, the capillary force in porous wick has to overcome a larger drag force, which leads to a decreaseing mass flow rate.

5.3 Effect of fin width

Figure 14 shows the effect of fin width vs. average synergy angle. It can be seen that with the increase of the ratio of fin width to whole segment length, l_{xf} /l_x, the average synergy angle decreases to a minimum value and increases afterwards. When l_{xf} /l_x = 0.5, the synergy angle reaches a minimum value, which means the heat transfer is furthest enhanced. Thereafter, with further increase of fin width, the width of vapor outlet decreases, which makes it more difficult for the vapor to enter the vapor groove. That is to say that flow and

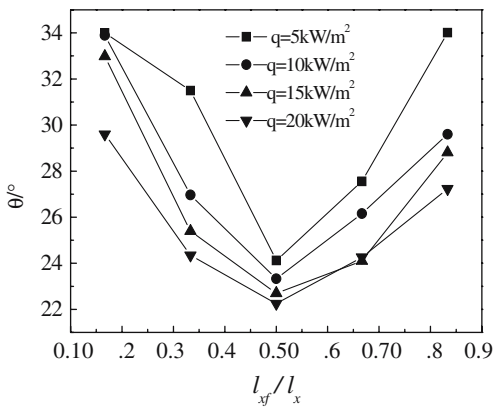

Fig. 14 Average synergy angle versus width of heating fin

heat transfer is not in good synergy and the synergy angle becomes large.

6 Conclusion

A numerical method is used to simulate the flow and heat transfer in the porous wick of a CPL evaporator under different heat fluxes for different geometrical data. The calculation results indicate that the heat flux and geometrical data, such as fin width and porous wick thickness, exert a great influence on flow and heat transfer of the evaporator. The study demonstrates that the field synergy principle can be applied to optimize the evaporator configuration and analyze heat transfer enhancement in the CPL evaporator.

Acknowledgments This work is supported by the National Key Basic Research Development Program of China (no. 2007CB206901).

References

1. Ku J, Swanson T, Herold K, Kolos K (1993) Flow visualization within a capillary evaporator. In: 23rd international conference on environmental systems. Colorado Springs, CO, 12–15 July 1993
2. Bazzo E, Riehl RR (2003) Operation characteristics of a small-scale capillary pumped loop. Appl Therm Eng 23(6):687–705
3. Chen P-C, Lin W-K (2001) The application of capillary pumped loop for cooling of electronic components. Appl Therm Eng 21:1739–1754
4. Ku J, Ottenstein L, Kob M et al. (2001) Temperature oscillations in loop heat pipe operation. In: EI-Genk MS (ed) Space technology and applications, international forum-STAIF 2001, pp 255–262
5. Muraoka I, Ramos FM, Vlassov VV (1998) Experimental and theoretical investigation of capillary pumped loop with a porous element in the condenser. Int J Heat Mass Transf 25(8):1085–1094
6. Cao YD, Faghri A (1994) Conjugate analysis of a flat-plate type evaporator for capillary pumped loops with three-dimensional vapor flow in the groove. Int J Heat Mass Transf 37(3):401–409
7. Demidov AS, Yatsenko ES (1994) Investigation of heat and mass transfer in the evaporation zone of a heat pipe operating by the 'inverted meniscus' principle. Int J Heat Mass Transf 37:2155–2163
8. Figus C, Le Bray Y, Bories S et al. (1999) Heat and mass transfer with phase change in a porous structure partially heated: continuum model and pore network simulation. Int J Heat Mass Transf 42:2557–2569
9. LaClair TJ, Mudawar I (2000) Thermal transient in a capillary evaporator prior to the initiation of boiling. Int J Heat Mass Transf 43(21):3937–3952
10. Guo ZY, Li DY, Wang BX (1998) A novel concept for convective heat transfer enhancement. Int J Heat Mass Transf 41(14):2221–2225
11. Tao WQ, Guo ZY, Wang BX (2002) Field synergy principle for enhancing convective heat transfer-its extension and numerical verifications. Int J Heat Mass Transf 45:3849–3856
12. Shen S, Liu W, Tao WQ (2003) Analysis of field synergy on natural convective heat transfer in porous media. Int Comm Heat Mass Transf 30(8):1081–1090
13. Liu W, Zhao XX (1998) 2D numerical simulation for simultaneous heat, water and gas migration in soil bed under different environmental conditions. Heat Mass Transf 34(4):307–316
14. Beckermann C, Viskanta R (1988) Natural convection solid/liquid phase change in porous media. Int J Heat Mass Transf 31(1):35–46
15. Liao Q, Zhao TS (1995) Evaporative heat transfer in a capillary structure heated by a grooved block. J Thermophys Heat Transf 38:3091–3101